Establishment of Gemcitabine-resistant Mouse Pancreatic Ductal Adenocarcinoma Cell Line and Possible Therapeutic Agents

Miyashita, Kumiko ; Yamashita, Kimihiro ; Miyoshi, Makoto ; Nishiyama, Takaaki ; Ise, Yuki ; Ohsaka, Shun ; Shimizu, Kazuya ; Nishimura,…

(Citation)
Anticancer Research,46(4):1819-1831

(Issue Date)
2026-04

(Resource Type)
journal article

(Version)
Version of Record

(URL)
https://hdl.handle.net/20.500.14094/0100503484

ANTICANCER RESEARCH *46*: 1819-1831 (2026)
doi: 10.21873/anticanres.18076

Establishment of Gemcitabine-resistant Mouse Pancreatic Ductal Adenocarcinoma Cell Line and Possible Therapeutic Agents

KUMIKO MIYASHITA[1], KIMIHIRO YAMASHITA[1], MAKOTO MIYOSHI[1], TAKAAKI NISHIYAMA[1], YUKI ISE[1], SHUN OHSAKA[1], KAZUYA SHIMIZU[1,2], NORIYUKI NISHIMURA[1] and YUICHI HORI[1]

[1]Department of Biophysics, Kobe University Graduate School of Health Sciences, Kobe, Japan;
[2]Department of Internal Medicine, Kobe Medical Center, Kobe, Japan

Abstract

Background/Aim: Pancreatic ductal adenocarcinoma (PDAC) remains highly lethal due to gemcitabine (GEM) resistance. This study aimed to establish a clinically relevant immunocompetent model to identify novel mediators of acquired GEM resistance.

Materials and Methods: Metastatic PDAC (mPDAC) cells, generated from CD133-positive pancreatic stem cells (mutant *Trp53, Cdk4, Kras*), were subjected to chronic *in vivo* GEM selection to establish a line with reduced sensitivity (mPDAC-R).

Results: mPDAC-R exhibited sustained growth under GEM treatment, alongside enhanced invasiveness and metastatic potential. Transcriptomic profiling identified monoamine oxidase B (MAOB) as an up-regulated mediator. Pharmacological inhibition of MAOB significantly suppressed proliferation and tumor growth in both mPDAC-R and human PDAC cell lines.

Conclusion: We established a novel GEM-resistant mPDAC model and identified MAOB as a promising therapeutic target. These findings provide a rationale for targeting MAOB-driven survival signals to overcome chemoresistance in refractory pancreatic cancer.

Keywords: Pancreatic ductal adenocarcinoma, gemcitabine resistance, CD133, cancer stem cell, monoamine oxidase B.

Introduction

Pancreatic ductal adenocarcinoma (PDAC) is highly lethal, with a 5-year survival rate of only 8.5% in Japan (1). Since most patients are diagnosed at advanced stages, the disease is frequently unresectable. For these patients, gemcitabine (GEM)-based chemotherapy remains the standard first-line treatment, used with or without surgical resection. Nevertheless, the rapid development of GEM resistance severely limits its clinical efficacy.

Yuichi Hori, MD, PhD, Department of Biophysics, Kobe University Graduate School of Health Sciences, Kobe, Japan. Tel/Fax: +81 787964540, e-mail: horiy@people.kobe-u.ac.jp

Received January 24, 2026 | Revised February 16, 2026 | Accepted February 20, 2026

Therefore, clarifying the molecular basis of GEM resistance is crucial for improving patient prognosis and developing effective second-line strategies.

Known mechanisms of GEM resistance include desmoplasia, impaired drug delivery due to poor vascularization, and reduced intracellular uptake (2). However, these mechanisms remain incompletely understood. A major challenge is that conventional xenograft models – typically involving the transplantation of human cells into immunodeficient mice – fail to reproduce key clinical features such as desmoplasia and distant metastasis. Consequently, there is an urgent need for experimental models that more accurately reflect the human tumor microenvironment.

Recently, a previous study reported the establishment of GEM-sensitive and GEM-resistant pancreatic cancer cells by introducing multiple cancer-related genes into normal human pancreatic ductal epithelial cells (3). Building on this approach, we aimed to develop a more clinically relevant experimental system. In this study, we established immunocompetent, *de novo* metastatic PDAC (mPDAC) cells derived from CD133-positive C57BL/6 mouse pancreatic stem cells, which effectively mimic desmoplasia and metastatic potential characteristic of human PDAC.

Transcriptomic analysis of parental and GEM-resistant cell lines identified monoamine oxidase B (MAOB) as a key mediator of GEM resistance. MAOB is an enzyme localized to the mitochondrial outer membrane that catalyzes the oxidative deamination of monoamines, a process that generates reactive oxygen species (ROS) (4). Furthermore, MAOB is known to be involved in the activation of cell survival signals, including the NF-κB pathway (5). While MAOB is a well-established target in neurodegenerative diseases, its role in cancer chemoresistance remains largely unexplored (6). Here, we show that MAOB-driven signaling contributes to tumor cell survival under chemotherapeutic stress, suggesting that targeting MAOB may represent a promising strategy to overcome GEM resistance in refractory pancreatic cancer.

Materials and Methods

Animals and ethical statement. All animal experiments were conducted in accordance with the Guidelines for the Care and Use of Laboratory Animals of Kobe University and were approved by the Institutional Animal Care and Use Committee (approval no. P200909). Male C57BL/6 and BALB/cAJc1-nu/nu mice (male, 6-10 weeks old) were purchased from CLEA Japan (Tokyo, Japan) and housed under specific-pathogen-free conditions with ad libitum access to food and water.

Cell line establishment and culture. Mouse gemcitabine sensitive metastatic pancreatic ductal adenocarcinoma cells (mPDAC-S) were established by introducing GFP, mutant Trp53, Cdk4, and mutant Kras into CD133-positive pancreatic progenitor cells isolated from embryonic day 12.5 (E12.5) mouse fetuses (7, 8). To establish a cell line with reduced GEM sensitivity, mPDAC-S cells were first transplanted subcutaneously into the flanks of C57BL/6 mice. Once tumors reached a detectable volume, the mice were subjected to chronic chemotherapy with GEM (100 mg/kg, intraperitoneally *i.p.*) administered twice weekly as a selection pressure. We monitored tumor volume and identified a specific tumor that exhibited sustained growth and eventually regrew on day 42 despite continuous treatment. This tumor was harvested, enzymatically dissociated, and the resulting cells were expanded *in vitro* to establish the gemcitabine resistant mPDAC (mPDAC-R) line. Human PDAC cell lines (KMC17, KMC26, and KMC34) were maintained as previously described (9).

In vitro phenotypic assays. Cell viability was assessed using the CCK-8 assay after 48 h of GEM treatment. *In vitro* invasiveness and migration were evaluated using Matrigel-coated Transwell inserts (24 h) and wound-healing assays (72 h), respectively. Organoid cultures were performed by suspending cells in Matrigel for five days. All *in vitro* assays were performed in triplicate and repeated in at least three independent experiments.

Table I. *List of primer sequences.*

Mouse primers		Sequence (5'->3')	Product length
CD133	Forward	CCTTGCCTCTTTGGACTCTG	439
	Reverse	CGGGCTTGTCATAACAGGAT	
Pdx1	Forward	CCGGACATCTCCCCATACGAA	509
	Reverse	GAGGTCACCGCACAATCTTGC	
MAOB	Forward	CTGGAACCTAGCAAGCAGCA	222
	Reverse	ATACGATTCTGGGTTGGCCC	
β-actin	Forward	GGCGGACTGTTACTGAGCTG	96
	Reverse	AAGCCATGCCAATGTTGTCTC	
Human primers		Sequence (5'->3')	Product length
MAOB	Forward	GCCCATGCACAGGATGAATTT	84
	Reverse	ACTAGGGAAGTGAGGCTATACAGG	
β-actin	Forward	AGCCTCGCCTTTGCCGATCC	104
	Reverse	TTGCACATGCCGGAGCCGTT	

In vivo tumor models and treatment. Tumorigenicity and metastatic potential were evaluated using three distinct transplantation models. For the subcutaneous model, cells were suspended 1:1 in Matrigel and injected into the flank of the mice. To more accurately recapitulate the primary tumor microenvironment, an orthotopic model was established *via* direct injection into the pancreatic tail. Furthermore, a metastasis model was utilized to assess the development of liver and lung lesions by injecting cells into the portal vein through the splenic hilum. Throughout the experiments, tumor growth was monitored by calculating volume using the formula (long axis×short axis^2)/2. To investigate the therapeutic efficacy of MAOB inhibition, mice were treated with oral rasagiline (15 mg/kg/day) administered twice weekly for a duration of 11-14 days following tumor confirmation (10).

Histological and molecular analyses. Paraffin-embedded sections were stained with Hematoxylin and Eosin (H&E), Alcian blue (for mucin), and AZAN (for fibrosis). Immunohistochemistry (IHC) was performed using antibodies against phosphorylated ERK, CD133, GFP, Ki67, and MAOB (11). Gene expression profiling was conducted using the Agilent Whole Mouse Genome Microarray (Agilent Technologies, Santa Clara, CA, USA) according to the manufacturer's protocol. mRNA levels were quantified *via* RT-PCR and qPCR, standardized to mouse or human *β-actin*. Primer sequences are listed in Table I. For protein analysis, mitochondrial fractions were isolated and analyzed *via* western blotting for MAOB, with COX IV as a loading control.

Statistical analyses. Data are presented as mean±SEM. Statistical significance was calculated using Student's *t*-test or two-way ANOVA and significance (*; **) is defined as $p<0.05$ or $p<0.01$, respectively. The specific number of subjects (n) for each experimental group is indicated in the respective figure legends.

Results

In vitro phenotype of mouse-derived artificial pancreatic cancer cells (gemcitabine-sensitive cell line; mPDAC-S). mPDAC-S cells expressed CD133 and Pdx1, indicating stem and progenitor cell characteristics (Figure 1A). GFP expression was detected using fluorescence microscopy (Figure 1B), and mutant p53 was localized to the nucleus by immunostaining (Figure 1C). KRAS activation was inferred from phosphorylated ERK, a downstream effector of RAS signaling (Figure 1D). GFP expression was also observed in colonies formed within organoids (Figure 1E

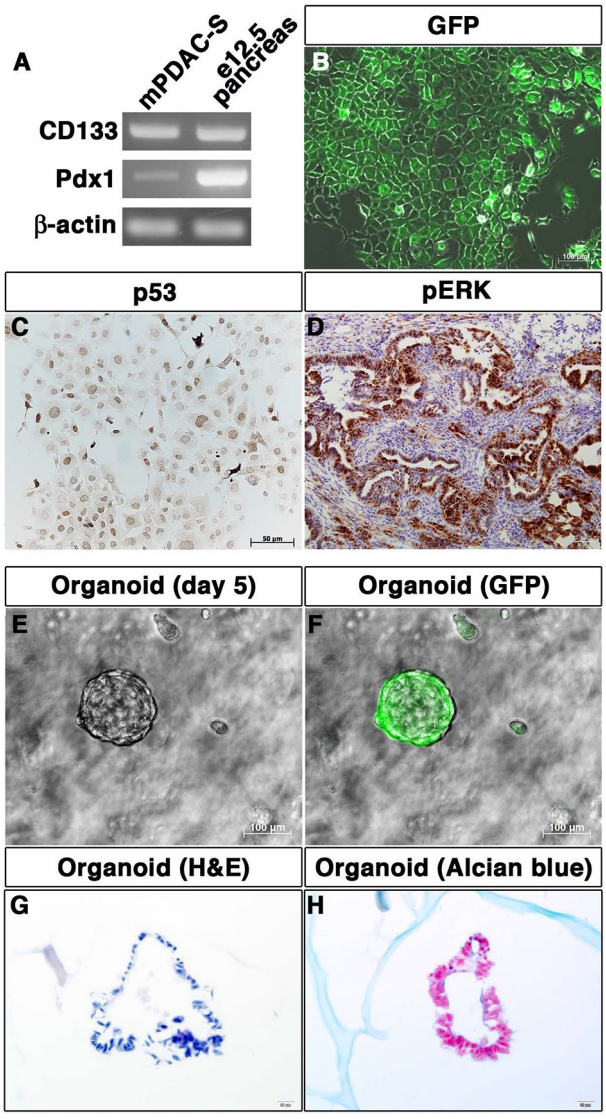

Figure 1. *In vitro characterization of mouse-derived, gemcitabine-sensitive metastatic pancreatic ductal adenocarcinoma cells (mPDAC-S). A) RT-PCR analysis showing expression of CD133 and Pdx1 in mPDAC-S cells; β-actin serves as a loading control. B, C) Immunofluorescence (IF) staining for GFP (B) and Immunocytochemical staining for mutant p53 (C) in mPDAC-S colonies. D) Immunohistochemical (IHC) staining for phosphorylated ERK, a downstream marker of KRAS signaling. E, F) Representative images of GFP-positive colonies in three-dimensional organoid cultures. G, H) Representative histological images of organoid structures stained with Alcian blue. Scale bars: 100 μm (B, E, F); 50 μm (C, D); 20 μm (G, H).*

and F). Alcian blue staining demonstrated mucus production within luminal structures of organoids (Figure 1G and H).

In vivo phenotype of mouse-derived artificial pancreatic cancer cells. mPDAC-S cells formed subcutaneous tumors within one month. Orthotopic transplantation of cells derived from these subcutaneous tumors into the pancreatic tail also led to tumor formation (Figure 2A). GFP expression confirmed the presence of cancer cells (Figure 2B). Histological analysis revealed mucin production (Figure 2C) and fibrosis (Figure 2D), features characteristic of human pancreatic cancer (12). Liver metastases were detected one month after orthotopic transplantation (n=3) (Figure 2E and F), and histology confirmed mucin production (Figure 2G) and fibrosis (Figure 2H).

Phenotype as cancer stem cells. CD133-positive mouse pancreatic stem cells were isolated using magnetic-activated cell sorting (MACS) and cultured, resulting in a mixed population of CD133-positive and CD133-negative cells (Figure 3A). Orthotopic transplantation of the isolated CD133-positive cells into the pancreas of BL6 mice led to tumor formation, in which GFP-positive cells comprised both CD133-positive and CD133-negative cells (Figure 3B). These results demonstrate that CD133-positive cells can generate heterogeneous tumor tissues, confirming their tumorigenic potential. They also suggest that tissue stem cells may serve as the origin of cancer stem cells.

Effect of GEM on mPDAC-S. The IC_{50} value of GEM for mPDAC-S was 0.08 μM (Figure 4A), indicating that the sensitivity of this cell line to GEM is higher than or comparable to that of established human pancreatic cancer cell lines (13). GEM has been reported to enhance the invasive ability of human cancer cells (14); therefore, we evaluated the effect of GEM on the invasion of mPDAC-S cells. *In vitro* Matrigel invasion assays demonstrated a significant increase in the number of invading cells following treatment with 0.1 μM GEM (Figure 4B). Cell migration area was also increased in a dose-dependent manner (n=3, p<0.05) (Figure 4C). *In vivo*, the effect of GEM on tumor growth was examined in subcutaneous and orthotopic pancreatic tumor models. Tumor growth was

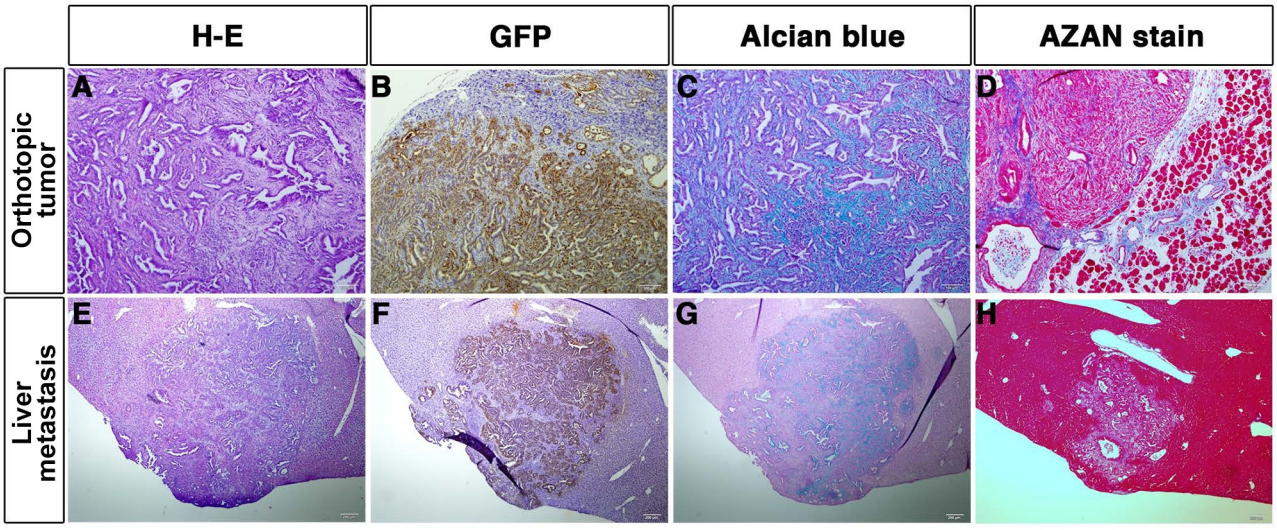

Figure 2. *In vivo histological characterization of orthotopic and metastatic gemcitabine-sensitive metastatic pancreatic ductal adenocarcinoma (mPDAC-S) tumors. A-D) Representative histological images of orthotopic mPDAC-S tumors stained with H&E (A), GFP (B), Alcian blue (C), and AZAN (D). E-H) Representative histological images of liver metastatic lesions stained with H&E (E), GFP (F), Alcian blue (G), and AZAN (H). Scale bars: 100 μm (A-D); 200 μm (E-H).*

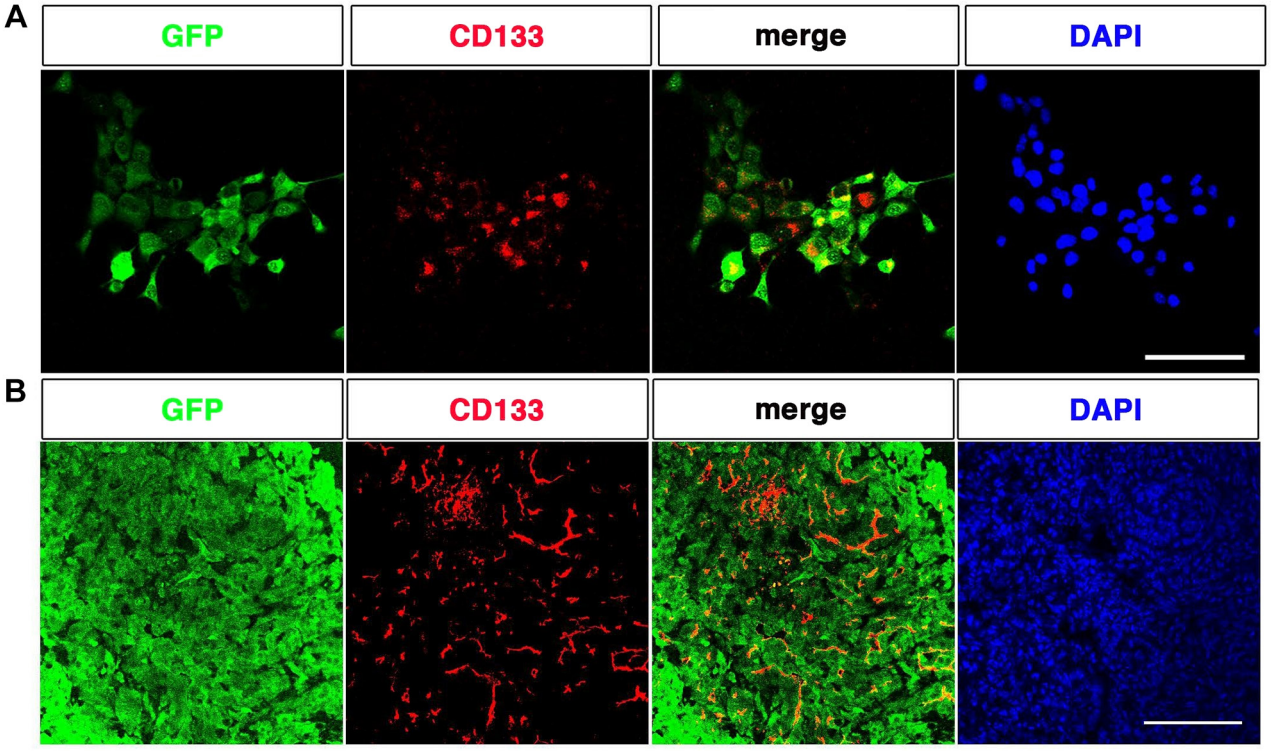

Figure 3. *CD133 expression in gemcitabine-sensitive metastatic pancreatic ductal adenocarcinoma (mPDAC-S) cells and tumors. A) Representative image of GFP, CD133, merged images, and DAPI in mPDAC-S cells. B) Representative images of GFP, CD133, merged images, and DAPI in mPDAC-S tumors. Scale bars: 100 μm.*

suppressed approximately two weeks after the start of GEM administration (Figure 4D and E), with tumor volumes of 657±101.5% in the control group *versus* 370±115.5% in the GEM-treated group (mean±SEM, n=4, p<0.05), and tumor weights of 1.125±0.2298 g *versus* 0.550±0.0353 g, respectively (mean±SEM, n=4, p<0.05). Histological analysis revealed that while tumors in the control group had clear boundaries, GEM-treated tumors exhibited invasion, with indistinct borders between the tumor and normal pancreatic tissue (Figure 4F).

Establishment of GEM-resistant cell line and effect of GEM on mPDAC-R. To establish a model with reduced GEM sensitivity, mPDAC-S cells were transplanted subcutaneously and treated with GEM. Although initial tumor growth was suppressed, a specific tumor exhibited definitive regrowth on day 42 (Figure 5A). This tumor was harvested to establish the mPDAC-R line.

The IC_{50} of GEM for mPDAC-R cells (30.0 μM) was higher than that for mPDAC-S cells, although this increase did not reach statistical significance *in vitro* (Figure 5B). However, *in vivo,* tumor growth was suppressed by GEM in mice transplanted with mPDAC-S, whereas tumors continued to grow in mice transplanted with mPDAC-R (Figure 5C), with tumor volumes of 2406±406.3% in the control group *versus* 442±108.3% in the GEM-treated group (mean±SEM, control, n=2; GEM-treated, n=2).

In vivo phenotype of mouse pancreatic cancer cells: mPDAC-S and mPDAC-R. Similar to mPDAC-S, mPDAC-R also formed pancreatic tumors one month after orthotopic transplantation. As shown in the collagen invasion assay, more mPDAC-R cells invaded than mPDAC-S cells (Figure 6A and B). Tumors derived from mPDAC-S exhibited distinct, swollen borders, whereas tumors derived from mPDAC-R displayed invasive growth into the surrounding pancreas (Figure 6C and D). The orthotopic pancreatic tumor volumes were comparable between the mPDAC-S group and the mPDAC-R group. In the metastasis model, liver metastases were observed within three weeks in all mice transplanted with either mPDAC-S (3/3) or mPDAC-R (4/4). mPDAC-S cells produced localized metastatic lesions confined to the liver, whereas mPDAC-R developed diffuse liver metastases accompanied by hepatomegaly (Figure 6E and F). Moreover, lung metastasis was detected in one of the four mice transplanted with mPDAC-R (1/4; Figure 6G). Similar to the primary tumors, metastatic lesions exhibited Alcian blue-positive mucin production and Azan-positive stromal fibrosis, both characteristic features of pancreatic ductal adenocarcinoma (Figure 7).

MAOB expression in mPDAC and tumor suppression effect of a MAOB inhibitor. Transcriptomic profiling and Gene Set Enrichment Analysis (GSEA) identified several differentially expressed genes related to drug metabolism. Among these, *Maob* was identified as the most highly up-regulated gene in mPDAC-R compared with mPDAC-S (Figure 8A). Expression of MAOB mRNA and protein was quantitatively confirmed by real-time PCR and western blotting and was significantly higher in mPDAC-R than in mPDAC-S (Figure 8B). As MAOB is localized to the mitochondrial outer membrane, immunostaining at the light microscope level showed cytoplasmic expression in both mPDAC-S and mPDAC-R cells (Figure 8C).

To evaluate the tumor-suppressive effect of the MAOB inhibitor rasagiline, subcutaneous tumors generated from mPDAC-R cells were treated for 11 days. Tumor volume in the rasagiline group was significantly reduced compared with the vehicle group on days 7 and 11 (Figure 8D). On day 11, tumor volume reached 389±123% in the vehicle group and 224±97% in the rasagiline group (mean±SEM, control vehicle, n=4; rasagiline-treated, n=4, p<0.01), relative to the baseline volume on day 0.

MAOB expression in GEM-resistant human pancreatic cancer cells and tumor suppression by a MAOB inhibitor. mRNA expression of MAOB was detected in KMC17, KMC26, and KMC34 cells using RT-PCR (Figure 9A), and MAOB protein was localized in the cytoplasm as determined by immunofluorescence staining (Figure 9B). Tumors generated by subcutaneous implantation of KMC26 and

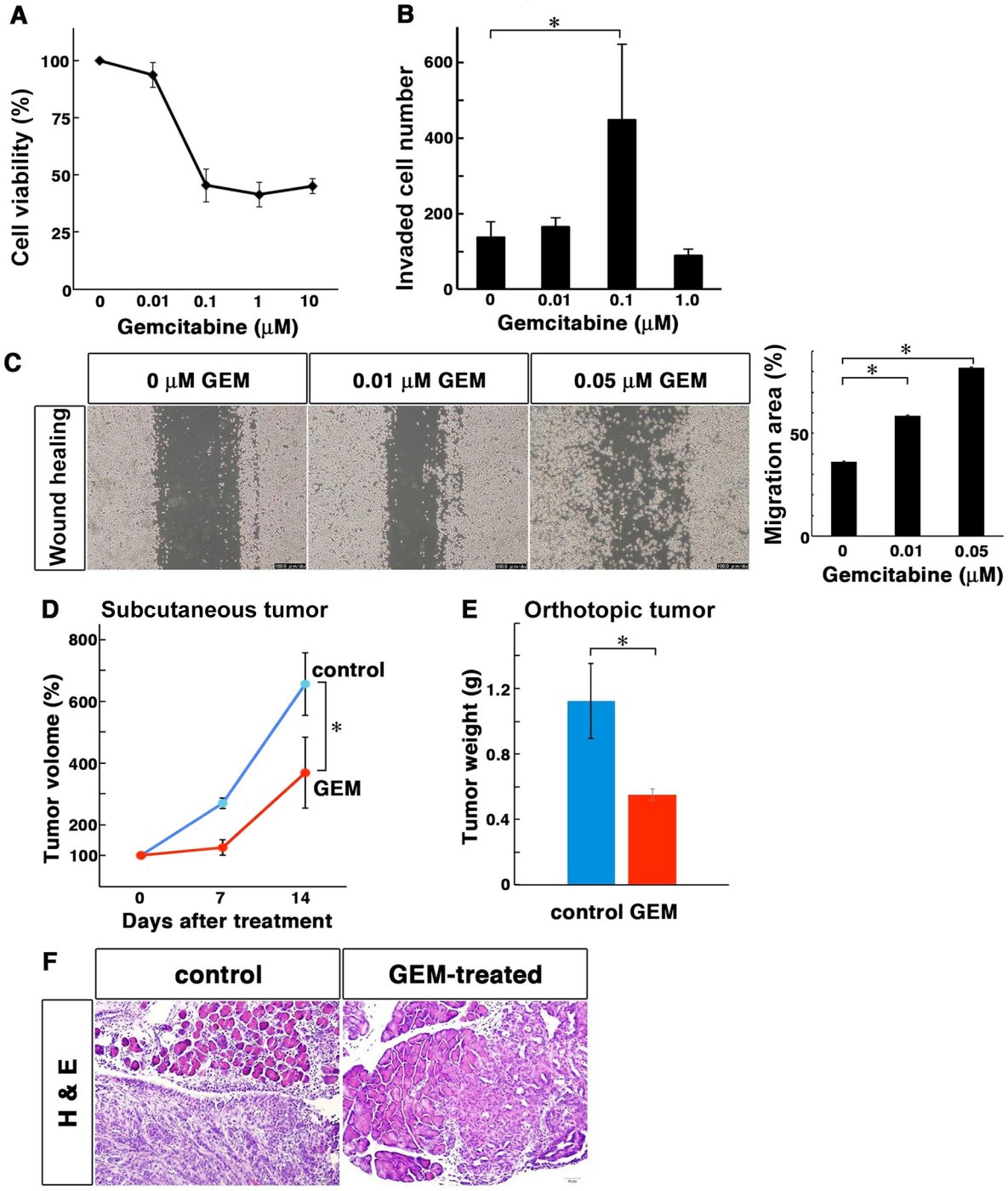

Figure 4. *Effects of gemcitabine on gemcitabine-sensitive metastatic pancreatic ductal adenocarcinoma (mPDAC-S) cells and tumors. A) Cell viability of mPDAC-S cells following gemcitabine treatment. B) Matrigel invasion assay of mPDAC-S cells treated with gemcitabine. C) Wound-healing assay showing migration of mPDAC-S cells after gemcitabine treatment. D) Growth curves of subcutaneous mPDAC-S tumors in vehicle- and gemcitabine-treated mice. Data represent mean±SEM (n=4 per group). *p<0.05. E) Weights of orthotopic mPDAC-S tumors in vehicle- and gemcitabine-treated mice. Data represent mean±SEM (n=4 per group). *p<0.05. F) Representative H&E-stained images of orthotopic mPDAC-S tumors from control and gemcitabine-treated groups. Scale bars: 100 μm (C); 50 μm (F).*

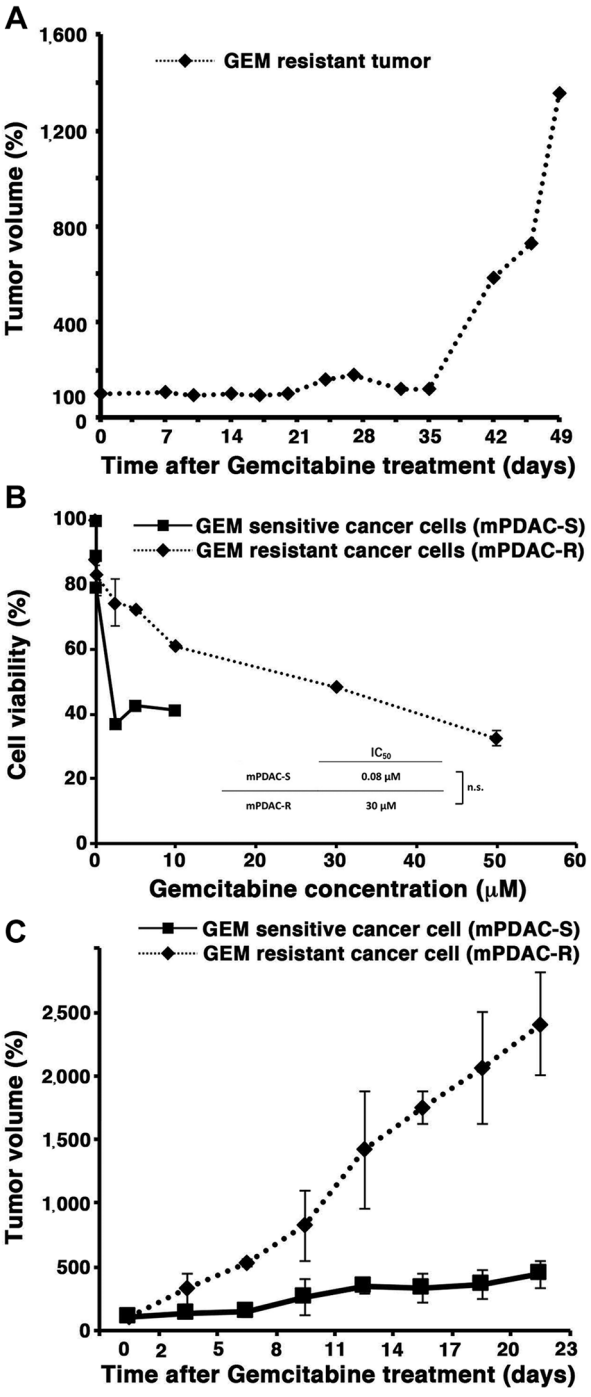

Figure 5. *Establishment and characterization of gemcitabine-resistant metastatic pancreatic ductal adenocarcinoma cells (mPDAC-R). A) In vivo establishment of gemcitabine (GEM) resistance. B) In vitro cell viability of mPDAC-S and mPDAC-R cells after GEM treatment. C) In vivo tumor growth comparison under GEM treatment (control, n=2; GEM-treated, n=2 per group). Data represent mean±SEM.*

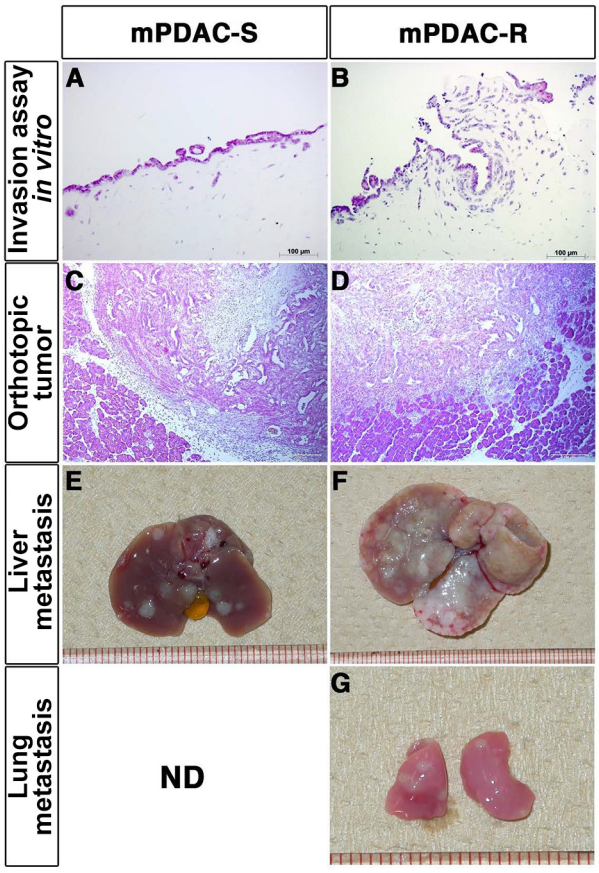

Figure 6. *Invasive and metastatic characteristics of gemcitabine-resistant metastatic pancreatic ductal adenocarcinoma (mPDAC-R). A, B) In vitro invasion assays shows increased invasiveness in mPDAC-R compared with mPDAC-S. C, D) Representative histological images stained with H&E shows expansive growth with well-defined borders in mPDAC-S (C) versus infiltrative morphology in mPDAC-R (D). E-G) In a splenic injection metastasis model, both lines formed liver metastases (mPDAC-S: n=3; mPDAC-R: n=4). Lung metastases is present only in the mPDAC-R group (1/4). GFP immunohistochemistry and histological staining confirmed metastatic lesions. Scale bars: 100 μm.*

KMC34 cells were treated with rasagiline for 13 days, and tumor volume was measured. Tumor volume in the rasagiline-treated group was significantly reduced compared with the vehicle group from day 3 after the start of treatment (Figure 9C). On day 13, tumor volume reached 557±63.7% in the vehicle group and 374±40% in the rasagiline group (mean±SEM, control vehicle, n=18; rasagiline-treated, n=17, p<0.01), relative to the baseline volume on day 0. Immunostaining of excised tumors with

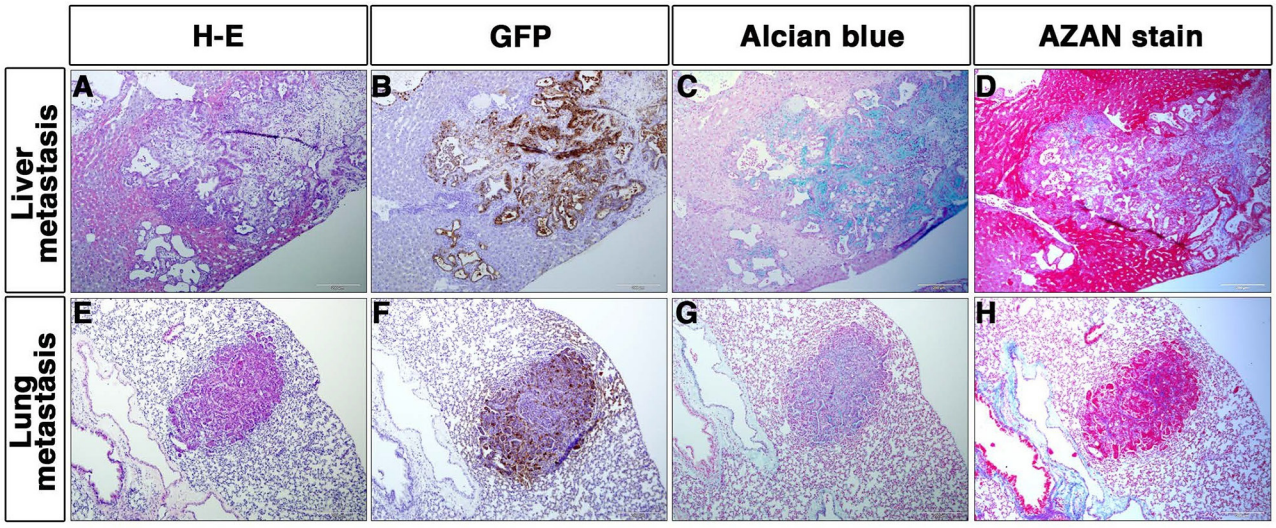

Figure 7. *Histological staining of liver and lung metastases derived from gemcitabine-resistant metastatic pancreatic ductal adenocarcinoma (mPDAC-R). A-H) Representative histological images stained with Alcian blue revealed mucus-producing cells in both liver (C) and lung (G) metastases. Azan staining demonstrated stromal fibrosis around metastatic lesions (D, H). Scale bars: 200 μm.*

an anti-Ki67 antibody showed that the percentage of Ki67-positive cells was significantly lower in the rasagiline-treated group (vehicle: 84±10% *vs*. rasagiline: 57±6%; n=3; mean±SEM, p<0.05; Figure 9D and E), confirming that MAOB inhibition directly suppresses the proliferative capacity of PDAC cells.

Discussion

In this study, we established a novel syngeneic PDAC model by introducing mutant *Trp53*, *Cdk4,* and mutant *Kras* into mouse CD133-positive pancreatic tissue stem cells. This orthotopic model rapidly mimics key human PDAC hallmarks – including desmoplasia and remote metastasis – within an immunocompetent environment. By comparing mPDAC-S and mPDAC-R cell lines through transcriptomic profiling, we identified MAOB as a novel mediator of GEM resistance. Additionally, pharmacological inhibition of MAOB by rasagiline also demonstrated tumor-suppressive effects against mPDAC-R, further supporting MAOB as a potential therapeutic target for refractory PDAC.

A key strength of this study is the use of a de novo mPDAC model derived from CD133-positive pancreatic stem cells (Figure 3). Given that pancreatic tissue stem cells are recognized as a potential cell of origin for PDAC (15), our model provides a biologically relevant framework that aligns with human tumorigenesis. Unlike conventional xenografts, this approach allows us to investigate drug resistance within a natural immune environment, further validating the clinical significance of MAOB as a mediator of GEM resistance.

Our *in vivo* observations using the mPDAC-S model demonstrate that while GEM treatment effectively reduced tumor burden, it simultaneously induced an invasive phenotype characterized by poorly defined tumor margins (Figure 4F). This suggests that prolonged GEM exposure exerts a potent selection pressure, favoring the survival and enrichment of sub-populations with enhanced migratory and invasive properties – a finding that aligns with our *in vitro* data (Figure 4B, C).We conclude that this continuous selection of aggressive clones eventually led to the establishment of mPDAC-R, which possesses both profound GEM resistance and high metastatic potential (16) (Figure 5A and C; Figure 6).

Intriguingly, the GEM resistance observed in our model appeared to be independent of classical metabolic

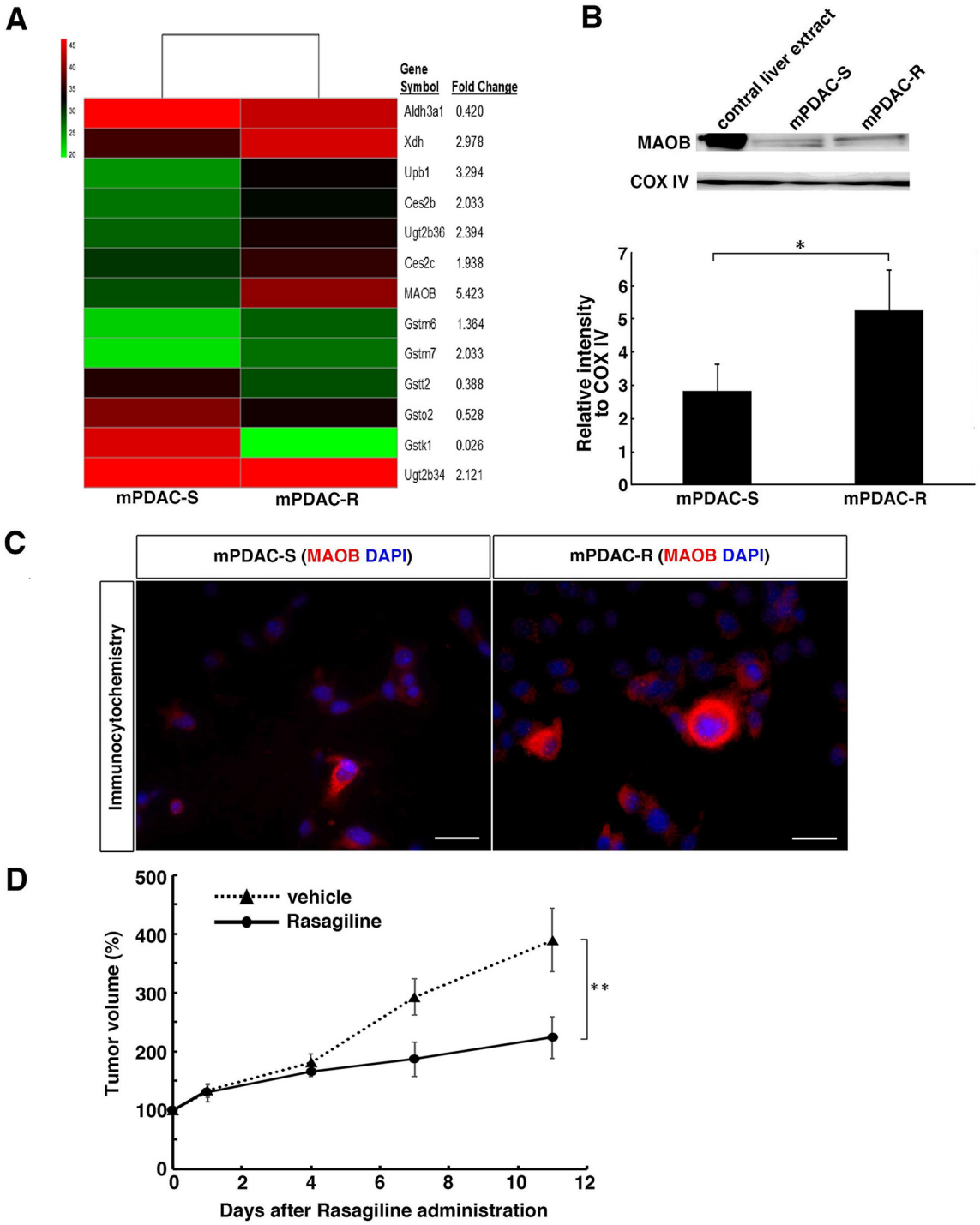

Figure 8. *Expression of monoamine oxidase B (MAOB) and the effect of Rasagiline in gemcitabine-resistant metastatic pancreatic ductal adenocarcinoma (mPDAC-R). A) Heatmap showing differential gene expression between mPDAC-S and mPDAC-R cells. B) Western blot analysis of MAOB expression in mitochondrial fractions of mPDAC-R and mPDAC-S; COX IV serves as a loading control. *p<0.05. C) Representative immunofluorescence images of MAOB expression in mPDAC-S and mPDAC-R cells. Scale bars: 100 μm. D) Growth curves of mPDAC-R tumors in mice treated with vehicle or rasagiline. Data represent mean±SEM. (n=4 per group). **p<0.01.*

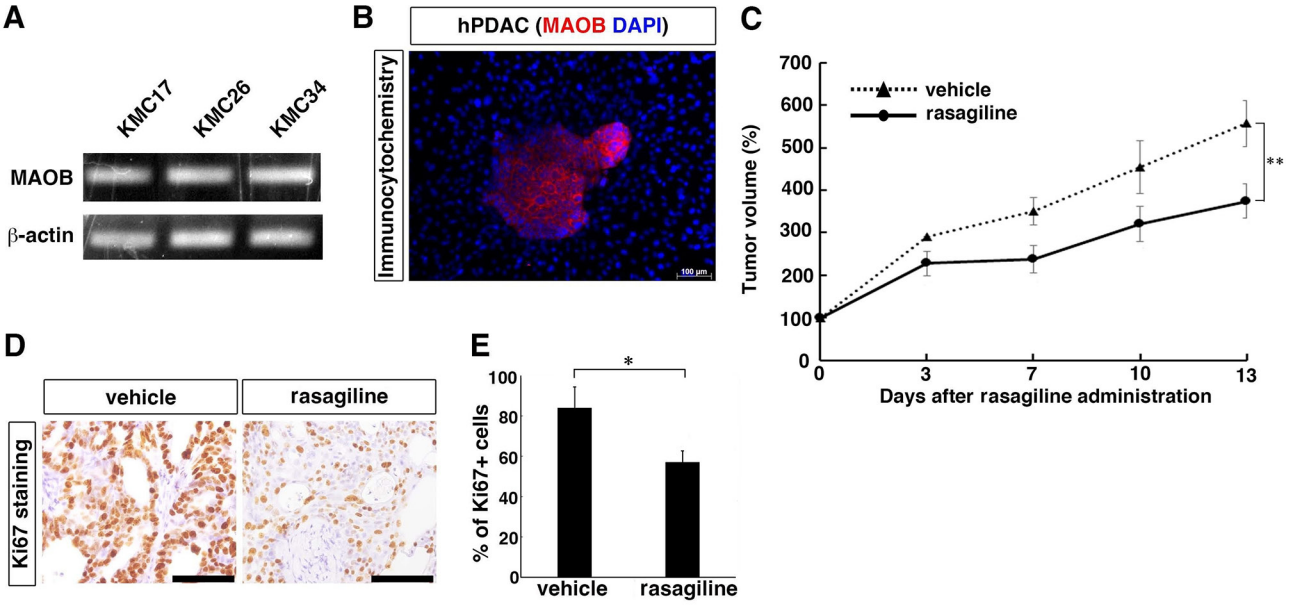

Figure 9. *MAOB expression and effect of rasagiline on human pancreatic ductal adenocarcinoma cells (hPDAC). A) RT-PCR analysis of MAOB expression in hPDAC cell lines (KMC17, KMC26, and KMC34). B) Representative immunofluorescence images of MAOB expression in hPDAC cells. C) Growth curves of hPDAC xenografts in mice treated with vehicle or rasagiline. Data represent mean±SEM. (vehicle control, n=18; rasagiline-treated, n=17). **p<0.01. D) Representative Ki67 immunohistochemical staining of tumors from vehicle- and rasagiline-treated groups. E) Quantification of Ki67-positive cells. *p<0.05. Scale bars: 100 μm (B, D).*

pathways. While acquired resistance is typically attributed to alterations in GEM-metabolizing enzymes or transporters (17), our transcriptomic profiling showed that these canonical markers remained largely unchanged. Instead, we identified a marked and specific up-regulation of *Maob* in mPDAC-R (Figure 8A). The MAOB-mediated generation of ROS provides a critical link between mitochondrial metabolic activity and the activation of pro-survival programs, such as NF-κB signaling, in GEM-resistant cells (5). This functional role is further supported by the observation that pharmacological inhibition of MAOB by rasagiline suppressed cell proliferation and reduced Ki67 positivity in both mPDAC-R and human PDAC cell lines (Figure 9A-E). Collectively, these findings suggest that GEM resistance in this model arises not from altered drug metabolism, but from MAOB-driven survival signals that enable tumor cells to maintain their proliferative capacity under chemotherapeutic stress. Clinically, the identification of MAOB as a mediator of GEM resistance is significant for treating refractory PDAC. While previous strategies have focused primarily on drug-metabolizing enzymes, our findings suggest that targeting MAOB-driven survival signals offers a new therapeutic approach. Specifically, the efficacy of rasagiline in our model indicates that MAOB inhibition could be used in combination with GEM to overcome resistance. This provides a new rationale for improving outcomes in patients with invasive, GEM-resistant disease. Consistent with this concept, integrated bioinformatic analyses of human PDAC transcriptomic datasets have identified novel targets such as LPAR5 and ACSL5 that are linked to disease progression and therapeutic response but fall outside classical drug metabolism pathways (18). In addition, in human pancreatic cancer cell lines, the transcriptional repressor BHLHE41 has been shown to restore GEM sensitivity by suppressing IGFBP4-mediated survival signaling, independent of GEM transport or metabolic activation (19). The convergence of these human clinical and *in vitro* findings with our murine

in vivo evidence further supports the therapeutic potential of targeting non-canonical resistance mechanisms in PDAC.

Study limitations. First, although our model mimics key features of PDAC, it may not fully capture the extreme complexity of the human tumor microenvironment (TME), particularly the diverse immune cell infiltration seen in patients. Second, the upstream mechanisms responsible for *Maob* up-regulation and the direct effects of its genetic manipulation on GEM sensitivity remain to be fully elucidated. Nevertheless, the absence of classical metabolic alterations in our models highlights MAOB as a promising target for overcoming GEM resistance. Future preclinical studies focusing on the causal link between MAOB dynamics and drug response will be essential to validate the clinical utility of this strategy.

Conclusion

In conclusion, this study established a novel GEM-resistant mPDAC model and identified MAOB as a key mediator of GEM resistance. These results highlight MAOB as a promising therapeutic target for overcoming chemoresistance in refractory pancreatic cancer.

Conflicts of Interest

The Authors have no conflicts of interest to declare in relation to this study.

Authors' Contributions

KM performed the experiments, analyzed the data, and drafted the manuscript. KY performed data analysis and manuscript writing. MM, TN, YI, and SO contributed to experimental procedures and data collection. KS contributed to the clinical relevance assessment using human PDAC cell lines. NN contributed to histological analyses. YH conceived and supervised the study, secured funding, and critically revised the manuscript. All Authors read and approved the final manuscript.

Acknowledgements

This work was supported by JSPS KAKENHI Grant Number 18K08705 and 21K08684 (Y.H) and 21K07099 (K.S).

Artificial Intelligence (AI) Disclosure

During the preparation of this manuscript, a large language model (ChatGPT, OpenAI) was used solely for language editing and stylistic improvements in select paragraphs. No sections involving the generation, analysis, or interpretation of research data were produced by generative AI. All scientific content was created and verified by the authors. Furthermore, no figures or visual data were generated or modified using generative AI or machine learning–based image enhancement tools.

References

1 Center for Cancer Control and Information Services, National Cancer Center: Cancer mortality from vital statistics in Japan, 2021. Monitoring of Cancer Incidence in Japan (MCIJ): Survival 2009-2011. Tokyo, Japan, National Cancer Center, 2020.

2 Koltai T, Reshkin SJ, Carvalho TMA, Di Molfetta D, Greco MR, Alfarouk KO, Cardone RA: Resistance to gemcitabine in pancreatic ductal adenocarcinoma: a physiopathologic and pharmacologic review. Cancers (Basel) 14(10): 2486, 2022. DOI: 10.3390/cancers14102486

3 Kobayashi-Ooka Y, Akagi T, Sukezane T, Yanagita E, Itoh T, Sasai K: Cultures derived from pancreatic cancer xenografts with long-term gemcitabine treatment produce chemoresistant secondary xenografts: Establishment of isogenic gemcitabine-sensitive and -resistant models. Pathol Res Pract 263: 155632, 2024. DOI: 10.1016/j.prp.2024.155632

4 Banerjee C, Tripathy D, Kumar D, Chakraborty J: Monoamine oxidase and neurodegeneration: Mechanisms, inhibitors and natural compounds for therapeutic intervention. Neurochem Int 179: 105831, 2024. DOI: 10.1016/j.neuint.2024.105831

5 Arfin S, Jha NK, Jha SK, Kesari KK, Ruokolainen J, Roychoudhury S, Rathi B, Kumar D: Oxidative stress in cancer cell metabolism. Antioxidants (Basel) 10(5): 642, 2021. DOI: 10.3390/antiox10050642

6 Liu Y, Li D, Xie C, Pan Y, Shi Q: Monoamine oxidase b in cancers: implications for therapeutics and prognosis. J Inflamm Res 18: 15555-15586, 2025. DOI: 10.2147/JIR.S541110

7 Hori Y, Fukumoto M, Kuroda Y: Enrichment of putative pancreatic progenitor cells from mice by sorting for

Prominin1 (CD133) and platelet-derived growth factor receptor β. Stem Cells 26(11): 2912-2920, 2008. DOI: 10.1634/stemcells.2008-0192

8 Sasai K, Sukezane T, Yanagita E, Nakagawa H, Hotta A, Itoh T, Akagi T: Oncogene-mediated human lung epithelial cell transformation produces adenocarcinoma phenotypes In Vivo. Cancer Res 71(7): 2541-2549, 2011. DOI: 10.1158/0008-5472.CAN-10-2221

9 Shimizu K, Chiba S, Hori Y: Identification of a novel subpopulation of tumor-initiating cells from gemcitabine-resistant pancreatic ductal adenocarcinoma patients. PLoS One 8(11): e81283, 2013. DOI: 10.1371/journal.pone.0081283

10 Meier-Davis SR, Dines K, Arjmand FM, Hamlin R, Huang B, Wen J, Christianson C, Shudo J, Nagata T: Comparison of oral and transdermal administration of rasagiline mesylate on human melanoma tumor growth *in vivo*. Cutan Ocul Toxicol 31(4): 312-317, 2012. DOI: 10.3109/15569527.2012.676119

11 Shimizu K, Nishiyama T, Hori Y: Gemcitabine enhances Kras-MEK–induced matrix metalloproteinase-10 expression via histone acetylation in gemcitabine-resistant pancreatic tumor-initiating cells. Pancreas 46(2): 268-275, 2017. DOI: 10.1097/MPA.0000000000000744

12 Feig C, Gopinathan A, Neesse A, Chan DS, Cook N, Tuveson DA: The pancreas cancer microenvironment. Clin Cancer Res 18(16): 4266-4276, 2012. DOI: 10.1158/1078-0432.CCR-11-3114

13 Zhao B, Qin C, Li Z, Wang Y, Li T, Cao H, Yang X, Li T, Wang W: Multidrug resistance genes screening of pancreatic ductal adenocarcinoma based on sensitivity profile to chemotherapeutic drugs. Cancer Cell Int 22(1): 374, 2022. DOI: 10.1186/s12935-022-02785-7

14 Xu BQ, Fu ZG, Meng Y, Wu XQ, Wu B, Xu L, Jiang JL, Li L, Chen ZN: Gemcitabine enhances cell invasion via activating HAb18G/CD147-EGFR-pSTAT3 signaling. Oncotarget 7(38): 62177-62193, 2016. DOI: 10.18632/oncotarget.11405

15 Lodestijn SC, van Neerven SM, Vermeulen L, Bijlsma MF: Stem cells in the exocrine pancreas during homeostasis, injury, and cancer. Cancers (Basel) 13(13): 3295, 2021. DOI: 10.3390/cancers13133295

16 Samulitis BK, Pond KW, Pond E, Cress AE, Patel H, Wisner L, Patel C, Dorr RT, Landowski TH: Gemcitabine resistant pancreatic cancer cell lines acquire an invasive phenotype with collateral hypersensitivity to histone deacetylase inhibitors. Cancer Biol Ther 16(1): 43-51, 2015. DOI: 10.4161/15384047.2014.986967

17 Saiki Y, Hirota S, Horii A: Attempts to remodel the pathways of gemcitabine metabolism: Recent approaches to overcoming tumours with acquired chemoresistance. Cancer Drug Resist 3(4): 819-831, 2020. DOI: 10.20517/cdr.2020.39

18 Li R, Yang T, Ren K, Li J, Nagakawa Y, Zeng Y, Natsuyama Y, Yi SQ: Identification of new potential targets for pancreatic ductal adenocarcinoma by integrated bioinformatic analysis. Anticancer Res 44(10): 4233-4250, 2024. DOI: 10.21873/anticanres.17254

19 Shii H, Minami K, Takeya R, Ikeda R: BHLHE41 enhances gemcitabine sensitivity of pancreatic cancer cells through IGFBP4 suppression. Anticancer Res 46(1): 213-226, 2026. DOI: 10.21873/anticanres.17936